Dai, Yunyun; Wang, Yadong; Das, Susobhan; Xue, Hui; Bai, Xueyin; Hulkko, Eero; Zhang, Guangyu; Yang, Xiaoxia; Dai, Qing; Sun, Zhipei

Electrical Control of Interband Resonant Nonlinear Optics in Monolayer MoS_2

Published in:
ACS Nano

DOI:
10.1021/acsnano.0c02642

Published: 28/07/2020

Document Version
Publisher's PDF, also known as Version of record

ACS NANO

www.acsnano.org

ARTICLE

Electrical Control of Interband Resonant Nonlinear Optics in Monolayer MoS_2

Yunyun Dai,* Yadong Wang, Susobhan Das, Hui Xue, Xueyin Bai, Eero Hulkko, Guangyu Zhang, Xiaoxia Yang, Qing Dai, and Zhipei Sun*

Cite This: *ACS Nano* 2020, 14, 8442–8448

Read Online

ACCESS | Metrics & More | Article Recommendations | Supporting Information

ABSTRACT: **Monolayer transition-metal dichalcogenides show strong optical nonlinearity with great potential for various emerging applications. Here we demonstrate the gate-tunable interband resonant four-wave mixing and sum-frequency generation in monolayer MoS_2. Up to 80% modulation depth in four-wave mixing is achieved when the generated signal is resonant with the A exciton at room temperature, corresponding to an effective third-order optical nonlinearity $|\chi^{(3)}_{eff}|$ tuning from (~12.0 to 5.45) × 10^{-18} m^2/V^2. The tunability of the effective second-order optical nonlinearity $|\chi^{(2)}_{eff}|$ at 440 nm C-exciton resonance wavelength is also demonstrated from (~11.6 to 7.40) × 10^{-9} m/V with sum-frequency generation. Such a large tunability in optical nonlinearities arises from the strong excitonic charging effect in monolayer transition-metal dichalcogenides, which allows for the electrical control of the interband excitonic transitions and thus nonlinear optical responses for future on-chip nonlinear optoelectronics.**

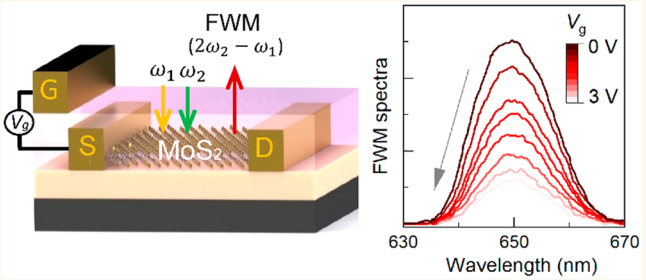

KEYWORDS: *nonlinear optics, four-wave mixing, sum-frequency generation, gate tunability, exciton, MoS_2*

Atomically thin transition-metal dichalcogenides (TMDs) have stimulated great interest due to their favorable physical properties,[1,2] such as extremely large exciton binding energy[3] and valley pseudospin physics arising from a large spin−orbit interaction.[4] In particular, TMD monolayers feature a direct band gap in the visible spectral range,[2,5] enabling diverse photonic applications including modulators,[6] photodetectors,[7] and light-emitting diodes.[8] Furthermore, TMD monolayers have recently attracted a surge of attention focusing on their fascinating optical nonlinearities[9] (*e.g.*, harmonic generation[10−12] and saturable absorption[13,14]), which are promising for various applications,[15] such as wavelength conversion[16,17] and ultrafast pulse generation.[18−20]

In TMD monolayers, the strongly bound and tunable excitons[3,21,22] enable the enhanced light−matter interaction[23,24] and tunable linear and nonlinear optical responses on the atomic thickness scale.[25,26] For example, it has been demonstrated that the strong interband excitonic effect results in the significant enhancement of various harmonic generation processes[27,28] in TMD monolayers. Additionally, it has been reported that second-harmonic generation in the WSe_2 monolayer can be electrically tuned at A-exciton resonance.[26] The interband excitonic enhancement and the tunability of nonlinear optical (NLO) responses are fascinating for numerous applications and will enable the versatility of future modern photonics, which is challenging with traditional NLO materials.[26,29−31] However, the electrical control of the other NLO responses in TMDs still remains unexplored, although it is highly desired for future applications.

In this work, we report the interband excitonic effect of various nonlinear optical processes, including four-wave mixing (FWM) and sum-frequency generation (SFG), in monolayer MoS_2 at room temperature. We fabricate an ion-gel-gated monolayer MoS_2 device for effective electron doping by applying positive gate voltages. We demonstrate the excitonic enhancement and the gate-tunable FWM of monolayer MoS_2. Similarly, for the SFG process, the enhancement and the nonlinear optical tunability at the interband excitonic resonance are also reported. Besides, the second- and third-order nonlinear coefficients are calculated as a function of doping carrier densities.

Received: March 28, 2020
Accepted: June 29, 2020
Published: June 29, 2020

https://dx.doi.org/10.1021/acsnano.0c02642
ACS Nano 2020, 14, 8442–8448

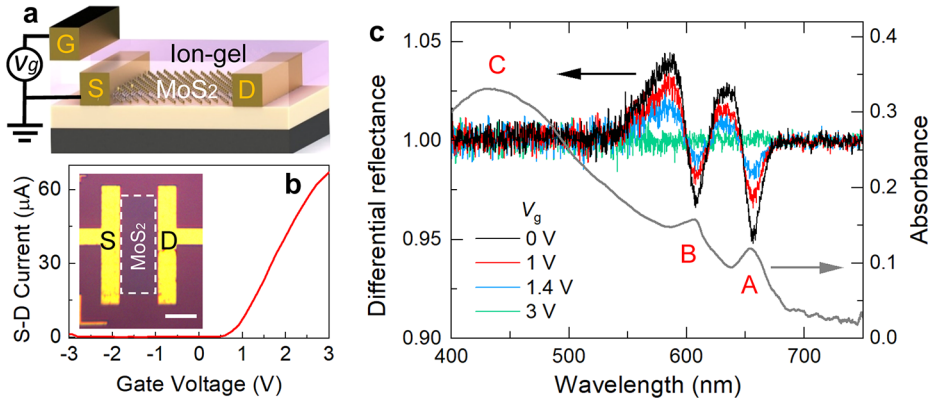

Figure 1. Monolayer MoS_2 device and its gate-tunable electrical and linear optical properties. (a) Schematic of the gated monolayer MoS_2 device with Ti/Au as source (S) and drain (D) electrodes. Ion gel is used as gate dielectric with Ti/Au as the gate (G) electrode. (b) Source-drain current of the MoS_2 device as a function of the gate voltage V_g from −3 to 3 V with the source−drain bias voltage fixed at 0.1 V. Inset: The optical image of the monolayer MoS_2 channel (white dashed box) with source−drain contacts (yellow regions) on the Si/SiO_2 substrate. Scaler bar: 20 μm. (c) Differential reflection spectra at different gate voltages and the reference linear absorption spectrum (gray) of monolayer MoS_2 at zero gate voltage. A, B, and C excitons are labeled.

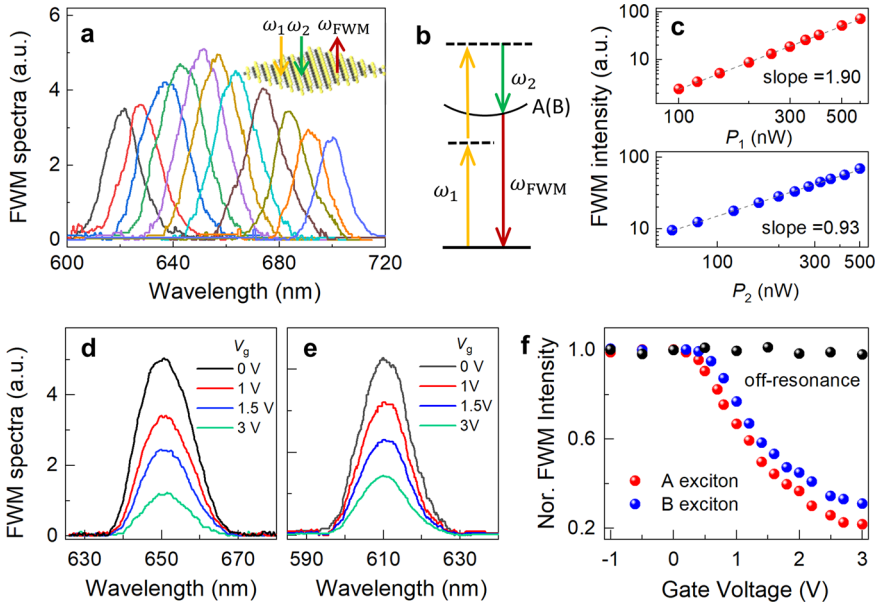

Figure 2. Gate-tunable FWM in monolayer MoS_2. (a) Wavelength-dependent FWM spectra. Pump λ_1 is at ~800 nm with an average power of ~1 μW, and idler λ_1 is tunable from ~930 to 1120 nm with an average power of ~1 μW. Inset: Schematic of the FWM of monolayer MoS_2. FWM (ω_{FWM}, red arrow) is generated from monolayer MoS_2 when it is excited by a pump light (ω_1, yellow arrow) and an idler light (ω_2, green arrow). (b) Diagram of the interband resonant FWM process with A(B) excitons. (c) Dependence of FWM peak intensities on incident light powers, with a fit of the experiment data to a power law I^s. Upper panel: Dependence of FWM on P_1 with fit (s = ~1.90). Lower panel: Dependence of FWM on P_2 with fit (s = ~0.93). (d) Gate-tunable FWM spectra resonant at the A exciton (~650 nm) with λ_1 = 800 nm and λ_2 = 1040 nm. (e) Gate-tunable FWM spectra resonant at the B exciton (~610 nm) with λ_1 = 800 nm, λ_2 = 1160 nm. (f) Normalized FWM peak intensities as a function of gate voltage for FWM resonant at the A- (650 nm, red dots) and B- (610 nm, blue dots) excitonic states and off-resonance (700 nm, black dots).

RESULTS AND DISCUSSION

Linear Optical Characterization in Monolayer MoS_2. A schematic and an optical image of the MoS_2 device are shown in Figure 1a,b. The device consists of a chemical-vapor-deposited (CVD) monolayer MoS_2 sheet on a SiO_2/Si substrate, with Ti/Au (5/50 nm) as the source and drain electrodes. The ion-gel top-gate method[32] is used for electrostatic gating, which changes the doping level and therefore the optical responses of MoS_2. By examination of the Raman and photoluminescence spectra (Figure S1), the CVD MoS_2 film is identified as a monolayer. Here the electrical property of monolayer MoS_2 is measured with different gate voltages. The transport curve is characteristic of an *n*-type semiconductor, as shown in Figure 1b. Over a gate voltage range (−3 to 3 V), the source−drain current increases with positive gating (*i.e.*, V_g > 0.4 V), indicating effective electron injection to MoS_2. The low off-current is due to the MoS_2-contact Schottky barrier.[33] Note that in our experimental range (*i.e.*, the gate voltage range is between −3 and 3 V), we are not able to obtain effective hole doping. Therefore, in the following experiments, we mainly study the device at positive gating with effective electron doping.

https://dx.doi.org/10.1021/acsnano.0c02642
ACS Nano 2020, 14, 8442−8448

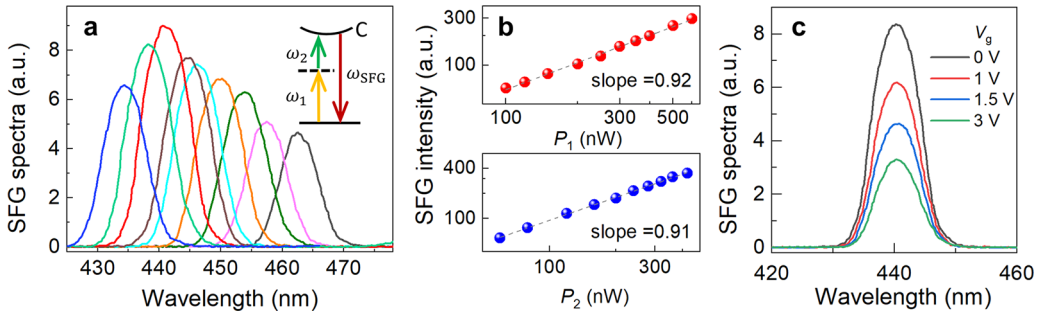

Figure 3. Gate-tunable SFG in monolayer MoS_2. (a) Wavelength-dependent SFG spectra. Inset: The diagram of interband resonant SFG (ω_{SFG}, red arrow) at the C exciton with excitations at ω_1 (yellow arrow) and ω_2 (green arrow). (b) Dependence of SFG peak intensities on incident powers, with a fit of the experiment data to a power law I^s. Upper panel: Dependence of SFG on P_1 with fit (s = ~0.92). Lower panel: Dependence of SFG on P_2 with fit (s = ~0.91). (c) Gate-tunable SFG spectra resonant at the C exciton (~440 nm) when λ_1 is at 800 nm and λ_2 is at 980 nm.

To understand the excitonic effect on the linear optical properties, the reflection spectra of the MoS_2 device are measured with electron doping at positive gating. The linear absorption spectrum of monolayer MoS_2 on a reference sapphire substrate shows pronounced absorption peaks attributed to A (~650 nm), B (~610 nm), and C (~440 nm) excitonic transitions with no electrostatic gating (gray curve in Figure 1c). However, at a large gate voltage (*e.g.*, V_g = 3 V with a doping carrier density of ~4 × 10^{13}/cm^2), the excitonic effect is strongly suppressed (Figure S2a). The carrier density is estimated using the capacitor model $N = C(V_g - V_{on})/e$, in which C is the ion-gel capacitance 2.45 μF/cm^2, e is the elementary charge, and V_{on} = 0.4 V is the turn-on voltage in the monolayer MoS_2 device.[32] Here we plot the differential reflection spectra $\frac{R(V_g) - R(3\ V)}{R(3\ V)}$ in Figure 1c, where $R(V_g)$ represents the reflection of the monolayer MoS_2 film on the Si/SiO_2 substrate at V_g. The differential reflection spectra clearly show a gate-tunable linear optical response at the A and B excitons. This is mainly because the injected carriers (*e.g.*, electrons when V_g > 0.4 V) decrease the oscillator strength of interband excitonic transitions:[25] The higher the positive gate voltage, the weaker the excitonic-transition-induced linear absorption will be. With a high enough gate voltage (*e.g.*, V_g = 3 V), the interband excitonic transitions could even be switched off while a lower energy resonance known as trion (*e.g.*, A-) emerges (Figure S2b).[34] The trion (A-) resonance is quite weak and is observable only by the derivative of the reflection spectra. Therefore, the influence of trion is insignificant in our experiments at room temperature. Note that a negligible change is observed at the C exciton, which is consistent with the result discussed in ref 25.

Gate Control of Interband Resonant FWM in MoS_2. A home-built femtosecond-laser-based microscopic system (Figure S3a) is employed for the nonlinear optical measurements in monolayer MoS_2, as described in the Methods section. The monolayer MoS_2 film, excited by two pump frequencies at ω_1 and ω_2 ($\omega_1 > \omega_2$), typically generates various nonlinear optical signals, for example, second-harmonic signals ($2\omega_1$ and $2\omega_2$), SFG ($\omega_1 + \omega_2$), and FWM ($2\omega_1 \pm \omega_2$, $\omega_1 \pm 2\omega_2$), as shown in Figure S4.

Here we mainly study the FWM generation (inset of Figure 2a): The pump light ($\hbar\omega_1$) is fixed at ~1.55 eV (*i.e.*, λ_1 = ~800 nm), and the idler light ($\hbar\omega_2$) is tunable in a near-infrared spectral range from ~1.1 to 1.33 eV (*i.e.*, λ_2 = ~930−1120 nm). As a result, the wavelength-dependent FWM (ω_{FWM} = $2\omega_1 - \omega_2$) from ~1.77 to 2.00 eV (*i.e.*, λ_{FWM} = ~620−700 nm) is studied, as shown in Figure 2a. The average power for both the pump and idler input light beams in the experiment is ~1 μW (with a corresponding peak intensity of ~44 GW/cm^2). We find that the FWM is enhanced at ~650 nm when the generated FWM photon energy (*i.e.*, $\hbar\omega_{FWM}$ = ~1.91 eV) matches the A-excitonic energy of monolayer MoS_2, suggesting the interband resonance at the A exciton (Figure 2b).

We further study the interband resonant FWM at the A exciton. Here we use a pump light ($\hbar\omega_1$) at ~1.55 eV (*i.e.*, λ_1 = ~800 nm) and an idler light ($\hbar\omega_2$) at ~1.19 eV (*i.e.*, λ_2 = ~1040 nm), and the generated FWM ($\omega_{FWM} = 2\omega_1 - \omega_2$) is at ~1.91 eV (*i.e.*, λ_{FWM} = ~650 nm). To examine the power dependence of the resonant FWM signal, the nonlinear optical spectra are measured when the power of the pump (P_1) and idler (P_2) light beams is changed, respectively. The upper panel of Figure 2c shows the peak intensities of the FWM spectra with increasing P_1 while P_2 = 1 μW. The lower panel of Figure 2c shows the peak intensities of FWM spectra with increasing P_2 while P_1 = 1 μW. It roughly follows a square and linear power-law behavior as a function of P_1 and P_2, respectively, which confirms the two-color FWM process ($\omega_{FWM} = 2\omega_1 - \omega_2$) involving the pump and idler light beams (details in the Supporting Information). We also study the gate-tunable resonant FWM in monolayer MoS_2 with interband A-excitonic resonance, as shown in Figure 2d. The FWM intensities decrease significantly when V_g changes from 0 to 3 V. We attribute the gate-tunable FWM to the modulation of the oscillator strength of the interband excitonic resonance by the gate-injected electrons.[26] With increasing gate voltages, the oscillator strength at the excitonic resonance decreases with increased doping (as shown in Figure 1c), thus suppressing the exciton enhancement of nonlinear processes.[26] As a result, the FWM signals decrease with increasing gate voltage at the excitonic resonant wavelength. Note that the gate-tunable FWM results are repeatable (Figure S5).

Similarly, with pump light ($\hbar\omega_1$) at ~1.55 eV (*i.e.*, λ_1 = ~800 nm) and idler light ($\hbar\omega_2$) at ~1.07 eV (*i.e.*, λ_2 = ~1160 nm), the generated FWM ($\omega_{FWM} = 2\omega_1 - \omega_2$) at ~2.03 eV (*i.e.*, λ_{FWM} = ~610 nm) is resonant with the B-excitonic state. Figure 2e shows gate-tunable resonant FWM spectra at the B exciton, where the FWM intensities also decrease with increased electrostatic doping due to the same operation principle.

https://dx.doi.org/10.1021/acsnano.0c02642
ACS Nano 2020, 14, 8442−8448

The normalized gate-tunable FWM ($\frac{I_{FWM}(V_g)}{I_{FWM}(0\ V)}$) is plotted in Figure 2f, where $I_{FWM}(V_g)$ is the peak intensity of FWM at V_g. Here we achieve a nearly 80% (70%) modulation depth ($\frac{|I_{FWM}(V_g) - I_{FWM}(0\ V)|}{I_{FWM}(0\ V)}$) when FWM is resonant at the A(B)-excitonic states with V_g tuning from 0 to 3 V. As a comparison, for the FWM at 700 nm (*i.e.*, λ_1 at 800 nm and λ_2 at 920 nm), which is off excitonic resonance, gating does not change the FWM intensity (black dots in Figure 2f). This further demonstrates the dominance of the interband excitonic effect on the optical nonlinearity of monolayer TMDs. Note that the FWM remains constant when $V_g < \sim 0.4$ V, which is due to the fact that the effective electron injection to MoS_2 has a turn-on threshold V_{on} at 0.4 V. This critical V_{on} is also indicated by the transport characteristics of monolayer MoS_2 (Figure 1b).

Gate Control of Interband Resonant SFG in MoS_2. We also use the home-built femtosecond-laser-based microscopic system to study SFG in monolayer MoS_2, as described in the Methods section. The SFG at the sum frequency ($\omega_{SFG} = \omega_1 + \omega_2$) is generated with the two input light beams at ω_1 and ω_2. In our SFG experiment, pump1 ($\hbar\omega_1$) is fixed at ~1.55 eV (*i.e.*, $\lambda_1 = \sim 800$ nm), and pump2 ($\hbar\omega_2$) is tunable in the near-infrared spectral range from ~1.11 to 1.33 eV (*i.e.*, $\lambda_2 = \sim 930-1120$ nm). As a result, wavelength-dependent SFG is achieved from ~2.66 to 2.88 eV (*i.e.*, $\lambda_{SFG} = \sim 430-465$ nm) (Figure 3a). We find that SFG is enhanced at ~440 nm, when the generated SFG photon energy (*i.e.*, $\hbar\omega_{SFG} = \sim 2.82$ eV) matches the C-excitonic energy of monolayer MoS_2 (inset of Figure 3a). The enhancement suggests that the interband excitonic transition at the C exciton significantly contributes to the enhanced SFG process. The power-dependent SFG signals are examined (Figure 3b). The peak intensities of the SFG spectra scale linearly with pump1 power P_1 (while pump2 power $P_2 = \sim 1$ μW) and P_2 (while $P_1 = \sim 1$ μW), respectively, following the linear power-law behavior of SFG.

We also study the gate-tunable SFG of MoS_2 with interband C-excitonic resonance. The peak intensities of the resonant SFG at 440 nm decrease with increased electrostatic doping (Figure 3c), showing a nearly 60% modulation depth ($\frac{|I_{SFG}(V_g) - I_{SFG}(0\ V)|}{I_{SFG}(0\ V)}$) at $V_g = 3$ V, where $I_{SFG}(V_g)$ is the peak intensity of SFG at V_g. This demonstrates the gate tunability of the SFG process in monolayer MoS_2.

Gate-Tunable Nonlinear Optical Coefficients. We have realized the tunability of nonlinear optical signals, which arises from the strong excitonic charging effects in monolayer MoS_2, allowing for exceptional control over the oscillator strengths at the excitonic resonances. On the basis of the measured tunable FWM and SFG intensities, we can estimate the tunability of nonlinear coefficients of MoS_2. The second- and third-order nonlinear coefficients $\chi^{(2)}$ and $\chi^{(3)}$ are calculated from the measured average powers of the incident light and the generated nonlinear optical signals as follows[35]

$$|\chi^{(2)}| = \frac{8n_S c}{\alpha_S \omega_S}\sqrt{\frac{\varphi f \tau_1 \tau_2 D_1^{\ 2} D_2^{\ 2} n_1 n_2 \varepsilon_0 c P_S}{\tau_S D_S^{\ 2} n_S P_1 P_2}} \quad (1)$$

$$|\chi^{(3)}| = \frac{8n_F c}{\alpha_F \omega_F}\frac{\varphi f \tau_1 D_1^{\ 2} n_1 \varepsilon_0 c}{P_1}\sqrt{\frac{\tau_2 D_2^{\ 2} n_2 P_F}{\tau_F D_F^{\ 2} n_F P_2}} \quad (2)$$

where $P_{(1,2,S,F)}$ represents the average power of the two incident pump beams and the generated SFG/FWM signals, $f = 2$ kHz is the repetition rate, $\tau_{(1,2,S,F)} = \sim 230$ fs is the estimated pulse duration of the pump light beams and the SFG/FWM signals, $D_{(1,2,S,F)} = \sim 2.5$ μm is the diameter of the laser spot with a Gaussian spatial profile, $n_{(1,2,S,F)} = \sim 4.2$ is refractive index of the material at the pump light frequencies and SFG/FWM frequencies,[25] $\alpha_S = 2$ for the two-color SFG process, $\alpha_F = 3$ for the two-color FWM process, and $\varphi = (\pi/\ln 2)^{3/2}/8$. Therefore, the effective bulk-like second- and third-order nonlinear coefficients of monolayer MoS_2 ($\chi^{(2)}_{eff}$, $\chi^{(3)}_{eff}$) can be obtained, $\chi^{(2)}_{eff} = \chi^{(2)}/t$ and $\chi^{(3)}_{eff} = \chi^{(3)}/t$, where $t = \sim 0.7$ nm is the thickness of the monolayer MoS_2. The detailed calibration and calculation method are discussed in the Supporting Information. The typical average power of two pump light beams is ~1 μW for each light beam. When the gate voltage varies from 0 to 3 V, corresponding to the carrier density change from 0 to ~4 × 10^{13}/cm^2, the SFG signal at the C exciton changes from ~2.5 to 1.0 pW, and the FWM signal changes from ~0.14 to 0.029 pW at the A exciton and from ~0.093 to 0.028 pW at the B exciton. Therefore, we obtain the gate-tunable $|\chi^{(2)}_{eff}|$ and $|\chi^{(3)}_{eff}|$ of monolayer MoS_2, as shown in Figure 4. The

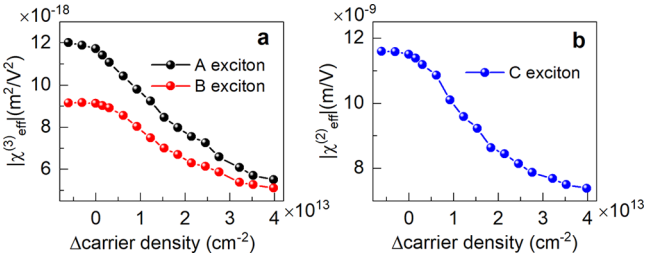

Figure 4. Gate-tunable nonlinear coefficients in monolayer MoS_2. (a) Gate-tunable $|\chi^{(3)}_{eff}|$ for FWM at the A and B excitons and (b) gate-tunable $|\chi^{(2)}_{eff}|$ for SFG at the C exciton.

tunability of $|\chi^{(3)}_{eff}|$ changes from (~12.0 to 5.45) × 10^{-18} m^2/V^2 at the interband A-excitonic resonance ((~9.16 to 5.03) × 10^{-18} m^2/V^2 at the interband B-excitonic resonance) as a function of the doping carrier density (Figure 4a). Similarly, the tunability of $|\chi^{(2)}_{eff}|$ with the interband C-exciton resonance at 440 nm changes from (~11.6 to 7.40) × 10^{-9} m/V with varying doping carrier density (Figure 4b).

The calculated second- and third-order nonlinear coefficients $|\chi^{(2)}_{eff}|$ and $|\chi^{(3)}_{eff}|$ are on the order of 10^{-9} and 10^{-18} m^2/V^2, which are in the same range of previously reported work (*e.g.*, $|\chi^{(2)}_{eff}| = \sim 5 \times 10^{-9}$ m/V in ref 36; $|\chi^{(3)}_{eff}| = \sim 10^{-17}$ to 10^{-19} m^2/V^2 in ref 12). Besides the electrical tunability, different approaches have been developed to tune nonlinear optical responses of TMDs. For example, the strain-[37,38] and plasmonic-antenna-[39] induced tunability of the nonlinear optical response has been studied in TMDs (fully discussed in the Supporting Information). For further improvement, integrating monolayer MoS_2 with waveguides,[40] optical fibers,[41] or optical cavities[31] will enhance light−matter interactions for higher light conversion efficiency. Besides, gate-tunable optical nonlinearity at low temperature offers the possibility for higher tunability and a better understanding of the underlying physics.[26]

CONCLUSIONS

The interband excitonic resonance of FWM and SFG is investigated in ion-gel-gated monolayer MoS_2 at room temperature. The gate-tunable interband excitonic FWM and

https://dx.doi.org/10.1021/acsnano.0c02642
ACS Nano 2020, 14, 8442−8448

SFG are demonstrated by electrostatic doping, which originates from the modulation of the oscillator strength of interband excitonic resonances. For interband resonant FWM, $|\chi^{(3)}_{eff}|$ of monolayer MoS_2 changes from (~12.0 to 5.45) × 10^{-18} m^2/V^2 at the A exciton (650 nm) and from (~9.16 to 5.03) × 10^{-18} m^2/V^2 at the B exciton (610 nm). Similarly, the tunability of $|\chi^{(2)}_{eff}|$ with the interband C-exciton resonance at 440 nm is tuned from (~11.6 to 7.40) × 10^{-9} m/V, with the gate voltage varying from 0 to 3 V. Note that a similar nonlinear optical tunability is anticipated for other TMDs (*e.g.*, WS_2). Therefore, our study is promising for electrically controlled NLO devices based on 2D layered materials (*e.g.*, tunable saturable absorbers,[42] on-chip nonlinear optics[43]), extending the versatility of modern photonic systems.

METHODS

MoS_2 Device Fabrication. The monolayer MoS_2 is grown on a SiO_2/Si substrate by the CVD method.[44] The source, drain and gate electrodes were first patterned using electron-beam lithography (Vistec) and then deposited with Ti/Au (5/50 nm) using electron-beam evaporation. All electrodes were wire-bonded to a chip for electrical control. Ion gel was spin-coated uniformly on the MoS_2 device. The ion-gel solution was prepared by dissolving 22 mg of poly(styrene)-*b*-poly(ethylene oxide)-*b*-poly(styrene) (PS−PEO−PS) and 0.56 g of ion liquid ([EMIM][TFSI]) in 20 mL of anhydrous dichloromethane.[32] The ion liquid and dry dichloromethane were purchased from Sigma-Aldrich, and PS−PEO−PS was purchased from Polymer Source.

Nonlinear Optical Spectra Measurement. A home-built femtosecond-laser-based microscopic system is employed for the nonlinear optical experiments. The schematic of this system is shown in Figure S3a. Two incident light beams, with different frequencies, are linearly polarized with polarization directions parallel to each other. Their typical spectra are shown in the Supporting Information. The pulse duration of the incident pulses is ~230 fs, which is estimated by the cross-correlation measurement (Figure S3c). The pulses of the two pump light beams are spatially and temporally overlapped and focused collinearly on the sample, and they generate the nonlinear optical signals in the monolayer MoS_2 film. The spectra of nonlinear optical signals are detected by a spectrometer (Andor, Hamamatsu) in the reflection configuration. The nonlinear optical signals of monolayer MoS_2 were measured under different gate voltages. Note that when different source−drain voltages were applied, no change was observed in nonlinear optical signals. Therefore, to fully exclude the electric-current-induced nonlinear optical effects (*e.g.*, current-induced second-order nonlinearity[45]), we only apply gate-voltage and ground source and drain electrodes (*i.e.*, no source−drain current) in our experiments.

ASSOCIATED CONTENT

Supporting Information

The Supporting Information is available free of charge at https://pubs.acs.org/doi/10.1021/acsnano.0c02642.

> MoS_2 film characterization, gate-tunable electrical and linear optical properties of monolayer MoS_2, FWM and SFG experiment setup and spectra of pump light, nonlinear optical spectra in monolayer MoS_2, the repeatable gate-tunable FWM, gate-tunable SFG spectra with excitonic resonance and off-resonance, calculation of nonlinear coefficients for SFG and FWM signals in MoS_2, wavelength-dependent third-order nonlinear coefficients of monolayer MoS_2, and comparison among different tuning approaches (PDF)

AUTHOR INFORMATION

Corresponding Authors

Yunyun Dai − *Department of Electronics and Nanoengineering, Aalto University, Fi-00076 Aalto, Finland;* orcid.org/0000-0002-1186-1864; Email: yunyun.dai@aalto.fi

Zhipei Sun − *Department of Electronics and Nanoengineering and QTF Centre of Excellence, Department of Applied Physics, Aalto University, Fi-00076 Aalto, Finland;* orcid.org/0000-0002-9771-5293; Email: zhipei.sun@aalto.fi

Authors

Yadong Wang − *Department of Electronics and Nanoengineering, Aalto University, Fi-00076 Aalto, Finland;* orcid.org/0000-0001-8603-3468

Susobhan Das − *Department of Electronics and Nanoengineering, Aalto University, Fi-00076 Aalto, Finland*

Hui Xue − *Department of Electronics and Nanoengineering, Aalto University, Fi-00076 Aalto, Finland*

Xueyin Bai − *Department of Electronics and Nanoengineering, Aalto University, Fi-00076 Aalto, Finland*

Eero Hulkko − *Department of Electronics and Nanoengineering, Aalto University, Fi-00076 Aalto, Finland*

Guangyu Zhang − *Institute of Physics and Beijing National Laboratory for Condensed Matter Physics, Chinese Academy of Sciences, Beijing 100190, China;* orcid.org/0000-0002-1833-7598

Xiaoxia Yang − *Division of Nanophotonics, CAS Center for Excellence in Nanoscience, National Center for Nanoscience and Technology, Beijing 100190, China*

Qing Dai − *Division of Nanophotonics, CAS Center for Excellence in Nanoscience, National Center for Nanoscience and Technology, Beijing 100190, China;* orcid.org/0000-0002-1750-0867

Complete contact information is available at: https://pubs.acs.org/10.1021/acsnano.0c02642

Author Contributions

Y.D. and Z.S. conceived the idea. Y.D. performed the experiments with assistance from Y.W., S.D., H.X., X.B., and E.H. on the device fabrication and characterization. G.Z., X.Y., and Q.D. provided the CVD-grown MoS_2 sample. Y.D. analyzed the experimental data. Y.D. and Z.S. wrote the manuscript with contributions from all authors.

Notes

The authors declare no competing financial interest.

ACKNOWLEDGMENTS

We acknowledge funding from the Aalto Centre for Quantum Engineering, Business Finland (A-Photonics), Academy of Finland (grant nos. 276376, 284548, 295777, 304666, 312297, 312551, and 314810), Academy of Finland Flagship Programme (grant no. 320167, PREIN), the European Union's Horizon 2020 research and innovation program (Grant No. 820423, S2QUIP), and ERC (grant no. 834742).

REFERENCES

(1) Manzeli, S.; Ovchinnikov, D.; Pasquier, D.; Yazyev, O. V.; Kis, A. 2D Transition Metal Dichalcogenides. *Nat. Rev. Mater.* **2017**, *2*, 17033.

(2) Mak, K. F.; Lee, C.; Hone, J.; Shan, J.; Heinz, T. F. Atomically Thin MoS_2: a New Direct-Gap Semiconductor. *Phys. Rev. Lett.* **2010**, *105*, 136805.

(3) He, K.; Kumar, N.; Zhao, L.; Wang, Z.; Mak, K. F.; Zhao, H.; Shan, J. Tightly Bound Excitons in Monolayer WSe_2. *Phys. Rev. Lett.* **2014**, *113*, 026803.
(4) Xu, X.; Yao, W.; Xiao, D.; Heinz, T. F. Spin and Pseudospins in Layered Transition Metal Dichalcogenides. *Nat. Phys.* **2014**, *10*, 343−350.
(5) Splendiani, A.; Sun, L.; Zhang, Y.; Li, T.; Kim, J.; Chim, C. Y.; Galli, G.; Wang, F. Emerging Photoluminescence in Monolayer MoS_2. *Nano Lett.* **2010**, *10*, 1271−5.
(6) Sun, Z.; Martinez, A.; Wang, F. Optical Modulators with 2D Layered Materials. *Nat. Photonics* **2016**, *10*, 227−238.
(7) Lopez-Sanchez, O.; Lembke, D.; Kayci, M.; Radenovic, A.; Kis, A. Ultrasensitive Photodetectors Based on Monolayer MoS_2. *Nat. Nanotechnol.* **2013**, *8*, 497−501.
(8) Sundaram, R. S.; Engel, M.; Lombardo, A.; Krupke, R.; Ferrari, A. C.; Avouris, P.; Steiner, M. Electroluminescence in Single Layer MoS_2. *Nano Lett.* **2013**, *13*, 1416−21.
(9) Autere, A.; Jussila, H.; Dai, Y.; Wang, Y.; Lipsanen, H.; Sun, Z. Nonlinear Optics with 2D Layered Materials. *Adv. Mater.* **2018**, *30*, No. 1705963.
(10) Autere, A.; Jussila, H.; Marini, A.; Saavedra, J. R. M.; Dai, Y.; Säynätjoki, A.; Karvonen, L.; Yang, H.; Amirsolaimani, B.; Norwood, R. A.; Peyghambarian, N.; Lipsanen, H.; Kieu, K.; de Abajo, F. J. G.; Sun, Z. Optical Harmonic Generation in Monolayer Group-VI Transition Metal Dichalcogenides. *Phys. Rev. B: Condens. Matter Mater. Phys.* **2018**, *98*, 115426.
(11) Karvonen, L.; Säynätjoki, A.; Huttunen, M. J.; Autere, A.; Amirsolaimani, B.; Li, S.; Norwood, R. A.; Peyghambarian, N.; Lipsanen, H.; Eda, G.; Kieu, K.; Sun, Z. Rapid Visualization of Grain Boundaries in Monolayer MoS_2 by Multiphoton Microscopy. *Nat. Commun.* **2017**, *8*, 15714.
(12) Saynatjoki, A.; Karvonen, L.; Rostami, H.; Autere, A.; Mehravar, S.; Lombardo, A.; Norwood, R. A.; Hasan, T.; Peyghambarian, N.; Lipsanen, H.; Kieu, K.; Ferrari, A. C.; Polini, M.; Sun, Z. Ultra-Strong Nonlinear Optical Processes and Trigonal Warping in MoS_2 Layers. *Nat. Commun.* **2017**, *8* (1), 893.
(13) Yan, P.; Chen, H.; Yin, J.; Xu, Z.; Li, J.; Jiang, Z.; Zhang, W.; Wang, J.; Li, I. L.; Sun, Z.; Ruan, S. Large-Area Tungsten Disulfide for Ultrafast Photonics. *Nanoscale* **2017**, *9*, 1871−1877.
(14) Chen, H.; Yin, J.; Yang, J.; Zhang, X.; Liu, M.; Jiang, Z.; Wang, J.; Sun, Z.; Guo, T.; Liu, W.; Yan, P. Transition-Metal Dichalcogenides Heterostructure Saturable Absorbers for Ultrafast Photonics. *Opt. Lett.* **2017**, *42*, 4279−4282.
(15) Wang, Q. H.; Kalantar-Zadeh, K.; Kis, A.; Coleman, J. N.; Strano, M. S. Electronics and Optoelectronics of Two-dimensional Transition Metal Dichalcogenides. *Nat. Nanotechnol.* **2012**, *7*, 699−712.
(16) Li, D.; Xiong, W.; Jiang, L.; Xiao, Z.; Rabiee Golgir, H.; Wang, M.; Huang, X.; Zhou, Y.; Lin, Z.; Song, J.; Ducharme, S.; Jiang, L.; Silvain, J. F.; Lu, Y. Multimodal Nonlinear Optical Imaging of MoS_2 and MoS_2-Based van der Waals Heterostructures. *ACS Nano* **2016**, *10*, 3766−75.
(17) Jakubczyk, T.; Delmonte, V.; Koperski, M.; Nogajewski, K.; Faugeras, C.; Langbein, W.; Potemski, M.; Kasprzak, J. Radiatively Limited Dephasing and Exciton Dynamics in $MoSe_2$ Monolayers Revealed with Four-Wave Mixing Microscopy. *Nano Lett.* **2016**, *16*, 5333−9.
(18) Mao, D.; Wang, Y.; Ma, C.; Han, L.; Jiang, B.; Gan, X.; Hua, S.; Zhang, W.; Mei, T.; Zhao, J. WS_2 Mode-Locked Ultrafast Fiber Laser. *Sci. Rep.* **2015**, *5*, 7965.
(19) Bonaccorso, F.; Sun, Z. Solution Processing of Graphene, Topological Insulators and Other 2D Crystals for Ultrafast Photonics. *Opt. Mater. Express* **2014**, *4*, 63−78.
(20) Zhang, H.; Bao, Q.; Sun, Z. Introduction to Two-Dimensional Layered Materials for Ultrafast Lasers. *Photonics Res.* **2018**, *6*, TDL1−TDL2.
(21) Ugeda, M. M.; Bradley, A. J.; Shi, S. F.; da Jornada, F. H.; Zhang, Y.; Qiu, D. Y.; Ruan, W.; Mo, S. K.; Hussain, Z.; Shen, Z. X.; Wang, F.; Louie, S. G.; Crommie, M. F. Giant Bandgap Renormalization and Excitonic Effects in a Monolayer Transition Metal Dichalcogenide Semiconductor. *Nat. Mater.* **2014**, *13*, 1091−5.
(22) Chernikov, A.; van der Zande, A. M.; Hill, H. M.; Rigosi, A. F.; Velauthapillai, A.; Hone, J.; Heinz, T. F. Electrical Tuning of Exciton Binding Energies in Monolayer WS_2. *Phys. Rev. Lett.* **2015**, *115*, 126802.
(23) Scuri, G.; Zhou, Y.; High, A. A.; Wild, D. S.; Shu, C.; De Greve, K.; Jauregui, L. A.; Taniguchi, T.; Watanabe, K.; Kim, P.; Lukin, M. D.; Park, H. Large Excitonic Reflectivity of Monolayer $MoSe_2$ Encapsulated in Hexagonal Boron Nitride. *Phys. Rev. Lett.* **2018**, *120*, 037402.
(24) Malard, L. M.; Alencar, T. V.; Barboza, A. P. M.; Mak, K. F.; de Paula, A. M. Observation of Intense Second Harmonic Generation from MoS_2 Atomic Crystals. *Phys. Rev. B: Condens. Matter Mater. Phys.* **2013**, *87*, 201401.
(25) Yu, Y.; Yu, Y.; Huang, L.; Peng, H.; Xiong, L.; Cao, L. Giant Gating Tunability of Optical Refractive Index in Transition Metal Dichalcogenide Monolayers. *Nano Lett.* **2017**, *17*, 3613−3618.
(26) Seyler, K. L.; Schaibley, J. R.; Gong, P.; Rivera, P.; Jones, A. M.; Wu, S.; Yan, J.; Mandrus, D. G.; Yao, W.; Xu, X. Electrical Control of Second-Harmonic Generation in a WSe_2 Monolayer Transistor. *Nat. Nanotechnol.* **2015**, *10*, 407−11.
(27) Wang, G.; Marie, X.; Gerber, I.; Amand, T.; Lagarde, D.; Bouet, L.; Vidal, M.; Balocchi, A.; Urbaszek, B. Giant Enhancement of the Optical Second-Harmonic Emission of WSe_2 Monolayers by Laser Excitation at Exciton Resonances. *Phys. Rev. Lett.* **2015**, *114*, 097403.
(28) Yoshikawa, N.; Nagai, K.; Uchida, K.; Takaguchi, Y.; Sasaki, S.; Miyata, Y.; Tanaka, K. Interband Resonant High-Harmonic Generation by Valley Polarized Electron-Hole Pairs. *Nat. Commun.* **2019**, *10*, 3709.
(29) Jiang, T.; Huang, D.; Cheng, J.; Fan, X.; Zhang, Z.; Shan, Y.; Yi, Y.; Dai, Y.; Shi, L.; Liu, K.; Zeng, C.; Zi, J.; Sipe, J. E.; Shen, Y.-R.; Liu, W.-T.; Wu, S. Gate-Tunable Third-Order Nonlinear Optical Response of Massless Dirac Fermions in Graphene. *Nat. Photonics* **2018**, *12*, 430−436.
(30) Soavi, G.; Wang, G.; Rostami, H.; Purdie, D. G.; De Fazio, D.; Ma, T.; Luo, B.; Wang, J.; Ott, A. K.; Yoon, D.; Bourelle, S. A.; Muench, J. E.; Goykhman, I.; Dal Conte, S.; Celebrano, M.; Tomadin, A.; Polini, M.; Cerullo, G.; Ferrari, A. C. Broadband, Electrically Tunable Third-Harmonic Generation in Graphene. *Nat. Nanotechnol.* **2018**, *13*, 583−588.
(31) Sun, Z. Electrically Tuned Nonlinearity. *Nat. Photonics* **2018**, *12*, 383−385.
(32) Chen, C. F.; Park, C. H.; Boudouris, B. W.; Horng, J.; Geng, B.; Girit, C.; Zettl, A.; Crommie, M. F.; Segalman, R. A.; Louie, S. G.; Wang, F. Controlling Inelastic Light Scattering Quantum Pathways in Graphene. *Nature* **2011**, *471*, 617−20.
(33) Kaushik, N.; Nipane, A.; Basheer, F.; Dubey, S.; Grover, S.; Deshmukh, M. M.; Lodha, S. Schottky Barrier Heights for Au and Pd Contacts to MoS_2. *Appl. Phys. Lett.* **2014**, *105*, 113505.
(34) Mak, K. F.; He, K.; Lee, C.; Lee, G. H.; Hone, J.; Heinz, T. F.; Shan, J. Tightly Bound Trions in Monolayer MoS_2. *Nat. Mater.* **2013**, *12*, 207−211.
(35) Boyd, R. W. The Nonlinear Optical Susceptibility. In *Nonlinear Optics*, 3rd ed.; Academic Press: New York, 2008.
(36) Kumar, N.; Najmaei, S.; Cui, Q.; Ceballos, F.; Ajayan, P. M.; Lou, J.; Zhao, H. Second-Harmonic Microscopy of Monolayer MoS_2. *Phys. Rev. B: Condens. Matter Mater. Phys.* **2013**, *87*, 161403.
(37) Liang, J.; Wang, J.; Zhang, Z.; Su, Y.; Guo, Y.; Qiao, R.; Song, P.; Gao, P.; Zhao, Y.; Jiao, Q.; Wu, S.; Sun, Z.; Yu, D.; Liu, K. Universal Imaging of Full Strain Tensor in 2D Crystals with Third-Harmonic Generation. *Adv. Mater.* **2019**, *31*, No. 1808160.
(38) Liang, J.; Zhang, J.; Li, Z.; Hong, H.; Wang, J.; Zhang, Z.; Zhou, X.; Qiao, R.; Xu, J.; Gao, P.; Liu, Z.; Liu, Z.; Sun, Z.; Meng, S.; Liu, K.; Yu, D. Monitoring Local Strain Vector in Atomic-Layered $MoSe_2$ by Second-Harmonic Generation. *Nano Lett.* **2017**, *17*, 7539−7543.
(39) Li, J.; Ji, Q.; Chu, S.; Zhang, Y.; Li, Y.; Gong, Q.; Liu, K.; Shi, K. Tuning the Photo-Response in Monolayer MoS_2 by Plasmonic Nano-Antenna. *Sci. Rep.* **2016**, *6*, 23626.

https://dx.doi.org/10.1021/acsnano.0c02642
ACS Nano 2020, 14, 8442−8448

(40) Alexander, K.; Savostianova, N. A.; Mikhailov, S. A.; Kuyken, B.; Van Thourhout, D. Electrically Tunable Optical Nonlinearities in Graphene-Covered SiN Waveguides Characterized by Four-Wave Mixing. *ACS Photonics* **2017**, *4*, 3039−3044.
(41) Chen, K.; Zhou, X.; Cheng, X.; Qiao, R.; Cheng, Y.; Liu, C.; Xie, Y.; Yu, W.; Yao, F.; Sun, Z.; Wang, F.; Liu, K.; Liu, Z. Graphene Photonic Crystal Fibre with Strong and Tunable Light-Matter Interaction. *Nat. Photonics* **2019**, *13*, 754−759.
(42) Bonaccorso, F.; Sun, Z.; Hasan, T.; Ferrari, A. C. Graphene Photonics and Optoelectronics. *Nat. Photonics* **2010**, *4*, 611−622.
(43) Ferrari, A. C.; Bonaccorso, F.; Fal'ko, V.; Novoselov, K. S.; Roche, S.; Boggild, P.; Borini, S.; Koppens, F. H.; Palermo, V.; Pugno, N.; Garrido, J. A.; Sordan, R.; Bianco, A.; Ballerini, L.; Prato, M.; Lidorikis, E.; Kivioja, J.; Marinelli, C.; Ryhänen, T.; Morpurgo, A.; et al. Science and Technology Roadmap for Graphene, Related Two-Dimensional Crystals, and Hybrid Systems. *Nanoscale* **2015**, *7*, 4598−810.
(44) Chen, W.; Zhao, J.; Zhang, J.; Gu, L.; Yang, Z.; Li, X.; Yu, H.; Zhu, X.; Yang, R.; Shi, D.; Lin, X.; Guo, J.; Bai, X.; Zhang, G. Oxygen-Assisted Chemical Vapor Deposition Growth of Large Single-Crystal and High-Quality Monolayer MoS_2. *J. Am. Chem. Soc.* **2015**, *137*, 15632−5.
(45) An, Y. Q.; Nelson, F.; Lee, J. U.; Diebold, A. C. Enhanced Optical Second-Harmonic Generation from the Current-Biased Graphene/SiO_2/Si(001) Structure. *Nano Lett.* **2013**, *13*, 2104−9.

https://dx.doi.org/10.1021/acsnano.0c02642
ACS Nano 2020, 14, 8442−8448